Li, T., Zhang, Y. & Hernández-Jiménez, F. (2016). Investigation of particle–wall interaction in a pseudo-2D fluidized bed using CFD-DEM simulations. *Particuology*, vol. 25, pp. 10-22.

DOI: 10.1016/j.partic.2015.06.001

Investigation of particle-wall interaction in a pseudo-2D fluidized bed using CFD-DEM simulations

Tingwen Li[a,b*], Yongmin Zhang[c], Fernando Hernández-Jiménez[d]

[a] National EnergyTechnologyLaboratory,Morgantown,WV26507,USA
[b] URS Corporation,Morgantown,WV26507,USA
[c] State Key Laboratory of Heavy Oil Processing, China University of Petroleum, Beijing 102249, China
[d] Universidad Carlos III of Madrid, Department of Thermal and Fluid Engineering, Av. de la Universidad, 30, 28911 Leganés, Madrid, Spain

Abstract

This paper reports discrete element method (DEM) simulations of a pseudo-two-dimensional (pseudo-2D) fluidized bed to investigate the particle-wall interaction. Detailed information of solids pressure and normal and tangential wall stresses are analyzed. It is found that the wall normal stress differs from the solids pressure due to the strong anisotropic flow behavior. There exists a simple linear relationship between the normal wall stress and the solids pressure. In addition, an effective friction coefficient can be derived for characterizing the particle-wall flow interaction. The conclusion has been confirmed by simulations with different particle stiffness. Finally, the assumptions in the newly developed model for 2D simulation by Li and Zhang (T. Li, Y. Zhang, A new model for two-dimensional numerical simulation of pseudo-2D gas–solids fluidized beds, Chem. Eng. Sci. 2013, 102:246–256) are examined against the DEM simulation.

Keyword: gas-solid flow, fluidized bed, computational fluid dynamics, discrete element method, particle-wall interaction, two-dimensional flow

1. Introduction

Pseudo-two dimensional (2D) fluidized beds, which are planar rectangular columns of limited thickness, are widely used in the experimental studies to better understand the complex flow dynamics in gas-solid systems. Benefit to the small thickness and typically transparent walls, they allow direct observation of the complex solids flow behavior such as bubble and clusters in gas-solid system through non-intrusive imaging techniques such as Particle Image Velocimetry (PIV) and Digital Image Analysis (DIA). Extensive fundamental research in pseudo-2D fluidized beds can be found in the literature on bubble properties, jet penetration, particle clustering, solids flow patterns, and solids mixing and segregation which have been utilized to improve the understanding of flow behavior in three-dimensional (3D) fluidized beds [1–14].

It is evident that the particle-wall interaction plays a significant role in affecting the flow behavior in gas-solid fluidized beds especially for lab-scale experimental systems and pseudo-2D systems. The front and back walls in a pseudo-2D fluidized bed restrict the solids movement in two directions and exert a strong friction to the solids flow which lead to quite different flow behaviors from a 3D cylindrical system [15–18]. However, in most numerical simulations, the pseudo-2D fluidized beds are modeled in two-dimension and the effect from the front and back walls are ignored. The wall effect in pseudo-2D gas-solid systems has been investigated in several numerical studies [19–23]. It has been demonstrated that the frictional effect from the front and back walls, which is not considered in most 2D simulations, leads to the deviation for solids velocity and bubble rising velocity [21–23]. To fully account for the effect of those walls, a 3D simulation is needed for accurate prediction of pseudo-2D gas-solid fluidized beds. Alternatively, Li and Zhang [24] developed a model for 2D simulations to account for the effect of front and back walls in a pseudo-2D gas-solid fluidized bed without the need of a 3D simulation. The results were clearly improved comparing to those obtained when the system was modelled just as a 2D plane, and the computational cost was greatly reduced compared to the 3D simulation.

There are several CFD modeling approaches for gas–solid flow simulations [25]. Among them, the Eulerian–Eulerian (EE) method (also called the two-fluid model or TFM), and the Lagrangian–Eulerian (LE) method are the most widely used approaches to simulate gas–solid flows. The former treats both gas and solid phases as interpenetrating continuum with appropriate constitutive correlations. The latter treats the gas phase as continuum, but tracks the solid phase on the particle level by solving the trajectory of each individual particle or swarm of particles. Specifically, the discrete element method (DEM), also known as discrete particle method (DPM), is often used in which the solid phase is represented by individual particles and particle-particle and particle-wall collisions are directly resolved using a hard-sphere or soft-sphere model. Given the detailed information provided by DEM simulations, it has been widely used to conduct fundamental research of granular flow to develop and validate the constitutive sub-model for the continuum model [26,27].

In the current study, DEM simulations of a pseudo-2D gas-solid fluidized bed are reported to investigate the particle-wall interaction. The numerical results of detailed particle-particle and particle-wall interactions are analyzed to derive the relationship between the field variables used in the TFM, specifically, solids pressure, normal and tangential stresses on the wall. Finally, the assumptions used in the 2D flow model proposed by Li and Zhang for pseudo-2D fluidized bed simulations are examined.

2. Numerical simulations

2.1. Numerical model

The open-source MFIX-DEM code, developed at US Department of Energy's National Energy Technology Laboratory (NETL) is used to conduct the numerical simulations of a 2D bubbling fluidized bed [28]. In MFIX-DEM, DEM for the solid particles is coupled with the CFD flow solver to simulate the gas-solid flow. For DEM, the inter-particle collisions are directly resolved using the soft-sphere model (based on a linear spring-dashpot model) of Cundall and Strack [29] which treats the collision as a continuous process taking place over a finite time. The contact force is then calculated as a function of the distance between colliding particles based on physically realistic interaction laws using empirical spring stiffness, dissipation constant, and friction coefficient. The particle–wall interaction is treated in the same way as the particle–particle collision. The gas flow is simulated by solving the averaged Navier-Stokes equations for mass and momentum conservation which account for solid volume fraction and additional coupling terms due to interactions between the two phases [30]. Details of the governing equations along with the numerical implementation, including the coupling procedure, can be found in [28]. The MFIX-DEM code has been verified and validated [31,32].

2.2. Simulated Setup

A pseudo-2D cold flow fluidized bed of dimensions 0.3 m × 1 m × 0.01 m is considered in the current study. Detailed information on the experimental setup and test can be found in [13]. The front and rear walls of the bed were made of glass for visual observation. Air at room temperature was fed through a perforated distributor to fluidize the bed material. The distributor consisted of two rows of 30 holes of diameter 1 mm arranged in a triangular configuration with 1 cm pitch. Experimental tests using the ballotini glass beads with density of 2500 kg/m^3 and sizes of 0.6-0.8 mm were simulated. The average particle diameter of 0.7 mm, which corresponds to the mean particle size, was used in the simulation.

A static bed height of 0.3 m which results in about 3 million particles inside the system was simulated. The bed is fluidized by air at a superficial gas velocity of 0.88 m/s which corresponds to two times the minimum fluidization velocity of 0.44 m/s. The numerical parameters used in the simulations are listed in Table 1. These parameters maintain constant for all simulations unless noted for the parametric study. A parametric study for the coefficient of friction for inter-particle and particle-wall collisions was carried out as it is believed to be the most critical parameter in the frictional forces of the walls acting on the particles. In addition, a parametric study for the particle spring constant was conducted to investigate its influence on the simulation results.

Table 1. Parameters used in the baseline numerical simulation.

Parameter	**Value**	**Parameter**	**Value**
Bed height, (m)	1	Bed width, (m)	0.3

Bed thickness, (m)	0.01	Static bed height, (m)	0.3
Particles density, (kg/m^3)	2500	Particle diameter, (mm)	0.7
Gas density, (kg/m^3)	1.2	Pressure, (atm)	1
Normal inter-particle spring constant, (N/m)	2000	Tangential inter-particle spring constant, (N/m)	571
Inter-particle restitution coefficient, (-)	0.95	Particle-particle frictional coefficient, (-)	0.6
Normal wall-particle spring constant, (N/m)	2000	Tangential wall-particle spring constant, (N/m)	571
Particle-wall restitution coefficient, (-)	0.8	Particle-wall frictional coefficient, (-)	0.6
Superficial gas velocity, (m/s)	0.88	Numerical grid size, (mm)	5

A uniform grid size of 5 mm is used for the CFD solver to discretize the 3D computational domain which leads to two cells in the thickness direction. Despite of the small thickness of a pseudo-2D system, multiple cells should be employed in the thickness direction of numerical simulations to have sufficient resolution for capturing the gradient in that direction. However, there exist several issues related to the DEM simulation if the dimension of computational cell is too small comparing to the particle size due to the large grid size required by the CFD–DEM coupling. Hence, the variation of gas flow in the thickness direction is ignored and a free-slip wall boundary condition is used for the gas phase at the front and rear walls. The wall effect is mainly accounted for by the solids flow through particle-wall interactions. Gas flow is fed through dispersed cells in the bottom boundary to mimic the perforated distributor used in the experiment. Limited by the grid resolution, 20 holes in the distributor were simulated to promote the bubble formation introduced by the jet collapsing observed in the experiment. The gas flow then leaves the computational domain through the top boundary at a constant pressure. A no-slip boundary condition is used for the gas phase at the left and right side walls.

All simulations were run in the hybrid parallel mode by coupling Distributed Memory Parallel (DMP) and Shared Memory Parallel (SMP) using Message Passing Interface (MPI) and OpenMP on NETL's supercomputer, HPCEE [33,34]. Transient simulation results were saved at a frequency of 100Hz and each simulation reached 10 seconds of physical time for analysis.

3. Results and discussion

3.1. Comparison to experimental observation

Figure 1 shows two snapshots taken from the experimental test and numerical simulation for qualitative comparison. In both figures, the light color corresponds to high solids concentration and dark color corresponds to bubble or freeboard with low solids

concentration. The small gas jets formed above the distributor orifices can be observed from the experimental image which is reasonably captured by the numerical simulation. Small bubbles formed near the distributor grow and collapse as they rise. Large bubbles finally burst at the bed surface. The numerical result shows smoother bubble surface than the experimental image mainly in the spherical capped region. The slight difference might be attributed to the particle size distribution in the bed material. Overall, the numerical simulation predicts reasonably agreeable bubbling behavior as observed in the experiment.

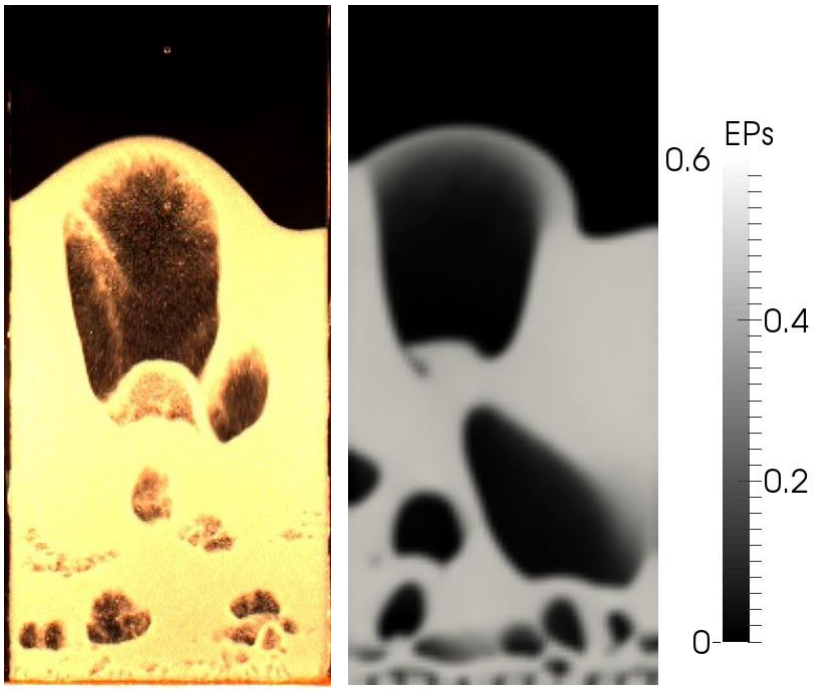

(a) (b)

Figure 1. Snapshots of solids distribution from (a) experiment and (b) numerical simulation (Numerical simulation: U_g=0.88 m/s, μ_{fric}=0.6).

In addition to the qualitative comparison to the experimental observation, the DEM simulation results have been used to characterize the overall wall frictional force [11]. Based on the force balance model proposed by Hernández-Jiménez et al. [13], the overall frictional force due to particle-wall interaction was estimated and found consistent with the experimental analysis. In addition, the DEM results corroborated that the overall frictional force can be considered equal to the velocity of the center of mass times a particle–wall interaction coefficient, *c*. Furthermore, a local estimation of the coefficient *c* was performed by analyzing the vertical component of the tangential force of the particle–wall collisions and the vertical particle velocity. It was found that the most probable value of the local coefficient *c* in the DEM simulations is similar to the global

value experimentally obtained. Given the qualitative and quantitative consistency to the experiment, the DEM simulation results reported in [11] are further analyzed to investigate the detailed particle-wall interaction in the pseudo-2D column.

3.2. Characterization of particle-wall interaction

To better understand the particle-wall interaction, the macroscopic flow variables typically used in the TFM, such as solids stress tensor, granular temperature, are extracted. To derive the continuous field variables from the DEM simulation results, appropriate spatial window size is needed for the data analysis. For the CFD-DEM simulation, it is natural to choose the fluid cell as the window for calculating the macroscopic field variables. By summing up the particle-wall contact force, $\mathbf{F}_{iW}$, for each particle in contact with the wall, the stress exerted by the particles on the wall can be calculated as

$$\mathbf{T}_W = \frac{1}{A}\sum_{i\in W}\mathbf{F}_{iw} \tag{1}$$

where A is the surface area of the wall cell.

The normal and tangential components of the wall stress are

$$T_n = \mathbf{n}\cdot\mathbf{T}_W \tag{2}$$

and

$$T_s = \left|\mathbf{T}_W - \mathbf{n}T_n\right| \tag{3}$$

where $\mathbf{n}$ is the unit vector normal to the wall.

The granular temperature, Θ, is calculated as

$$\Theta = \frac{1}{3N}\sum_{i=1}^{N}(\mathbf{u}_i - \bar{\mathbf{u}})\cdot(\mathbf{u}_i - \bar{\mathbf{u}}) \tag{4}$$

where N is the number of particle in the computational cell, m_i is the mass of particle, $\mathbf{u}_i$ is the particle velocity vector, and $\bar{\mathbf{u}}$ is the mean solids velocity in the cell. The macroscopic solid stress tensor, $\boldsymbol{\sigma}$, is calculated in each computational cell as [35]

$$\boldsymbol{\sigma} = \frac{1}{V}\sum_{i=1}^{N}\left[\sum_{j\neq i}\frac{1}{2}\mathbf{r}_{ij}\mathbf{F}_{ij} + m_i\left(\mathbf{u}_i - \bar{\mathbf{u}}\right)\left(\mathbf{u}_i - \bar{\mathbf{u}}\right)\right] \tag{5}$$

where $\mathbf{r}_{ij}$ is the vector from center of particle j to center of particle i and $\mathbf{F}_{ij}$ is the contact force between the colliding particles, and V is the volume of the domain for analysis, i.e. the computational cell. The solids pressure defined as the average of the diagonal terms of the solids stress tensor, i.e. $P_s = 1/3\left(\sigma_{11}+\sigma_{22}+\sigma_{33}\right)$ can be calculated as

$$P_s = \frac{1}{3V}\sum_{i=1}^{N}\left[\sum_{j\neq i}\frac{1}{2}\mathbf{r}_{ij}\cdot\mathbf{F}_{ij}\right] + \rho_p \varepsilon_s \Theta \tag{6}$$

The first term of Eq. (6) originates from the particle-particle interactions in form of instantaneous collision or long-time frictional contact. The second term stands for the kinetic contribution to the solids pressure [36]. It should be noted that the calculated quantities might be affected by the number of particles inside the sampling window. For example, granular temperature and solids pressure might demonstrate substantial statistical error for cells inside a bubble or in the freeboard region due to the limited number of particles there. In the current study, we mainly focus on the dense emulsion phase for which the number of particles in a computational cell is believed to be sufficient for the calculation [37].

Figure 2 shows the transient snapshots of the calculated field variables. Figure 2(a) presents the solids concentration distribution inside the bed. The solids pressure calculated based on Eq. (6) is shown in Figure 2(b) and the kinetic contribution i.e. the second term in the right-hand side of Eq. (6), is shown in Figure 2(c). As can be seen from these figures, the solids pressure is high in the dense emulsion phase and low in the dilute bubble region. Due to higher solids velocities and stronger solids interactions, the solids pressure in the bubble wake is especially higher than other areas. The kinetic component of solids pressure is mainly in the lower bubble wake area where the granular temperature as shown in Figure 2(f) is high. As revealed by the simulations, the kinetic part of solids pressure shown in Figure 2(c) is negligible comparing to the first part in equation (6). In the following analysis, the kinetic part of the solids pressure is ignored and only the component from inter-particle contacts is used. The normal and tangential components of the stress on the wall exerted by the particles are shown in Figure 2(d) and 2(e). From the transient snapshots, it can be seen that there tends to be a strong correlation between the solids pressure and the stress on the wall.

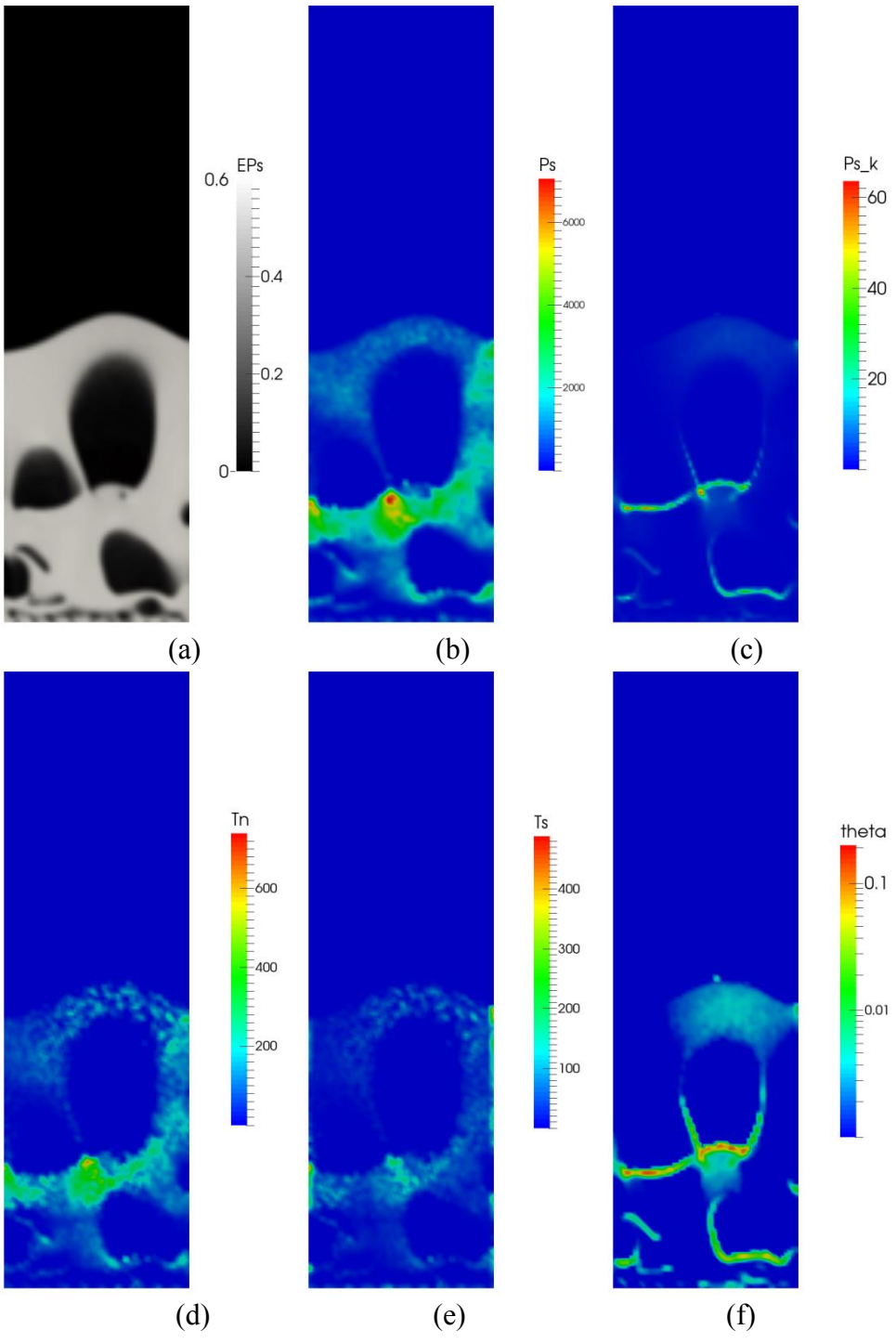

Figure 2. Snapshots of different field variables (a) solids concentration, (b) solids pressure, (c) kinetic contribution to the solids pressure, (d) normal wall stress, (e) tangential wall stress, (f) granular temperature. (Numerical simulation: U_g=0.88m/s, μ_{fric}=0.6).

In the following analysis, mainly the particle-wall interaction for the emulsion phase is investigated. For this purpose, the solids pressure and wall stresses in each computational cell are extracted for the emulsion phase. To distinguish the emulsion phase and the bubble phase, a voidage of 0.7 is used. A large amount of data has been extracted from the transient simulation results covering hundreds of frames for analysis. Figure 3 plots the values of normal wall stress versus the solids pressure for each computational cell collected over a 4 s simulation period. As can be seen, the normal wall stress demonstrates clear dependence on the solids pressure. The calculated normal wall stress increases with the solids pressure. According to the definition, the normal wall stress equals to σ_{33} at the wall which is the solids stress component in the normal wall direction. Hence, the difference between normal wall stress and the solids pressure shown here indicates the strong anisotropy in the flow. In particular, the normal wall stress is of the order of 7% of the solids pressure. The anisotropic flow behavior is believed to be related to gravitation, dominant flow direction, and wall effect. Clearly, the particle movement in the thickness direction is limited because of the wall effect and is less vigorous comparing to the other two directions. Hence the normal force on the wall exerted by the particle flow is much lower comparing to the solids pressure which is the average of three orthogonal normal stresses.

A simple linear regression is used to derive the relationship between these two variables as shown in the figure. The reported R-Square of 0.8161 indicates the linear fitting reasonably captures the correlation between normal wall stress and the solids pressure. Despite the apparent high scattering, most of the points are concentrated near the regression line.

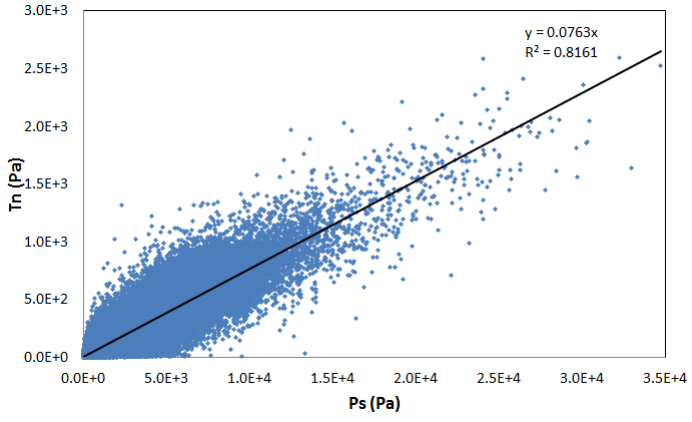

Figure 3. Normal wall stress versus solids pressure for the emulsion phase together with a linear regression (Numerical simulation: U_g=0.88m/s, μ_{fric}=0.6).

To further investigate the anisotropic flow behavior encountered in the current pseudo-2D system. The granular temperature is decomposed into three components

$$\Theta = \Theta_x + \Theta_y + \Theta_z \tag{7}$$

where Θ_x, Θ_y, and Θ_z account for the contribution from different velocity components. As shown in Figure 4, the magnitudes of different components of granular temperature are different. Most of granular temperature originates from the fluctuating velocity in the vertical direction which is the dominant flow direction. The presence of front and back walls confines the particle movement as well as its fluctuation in the thickness direction. Hence, the granular temperature contributed by the fluctuating solids velocity in the thickness direction is much less than those from the vertical and horizontal directions.

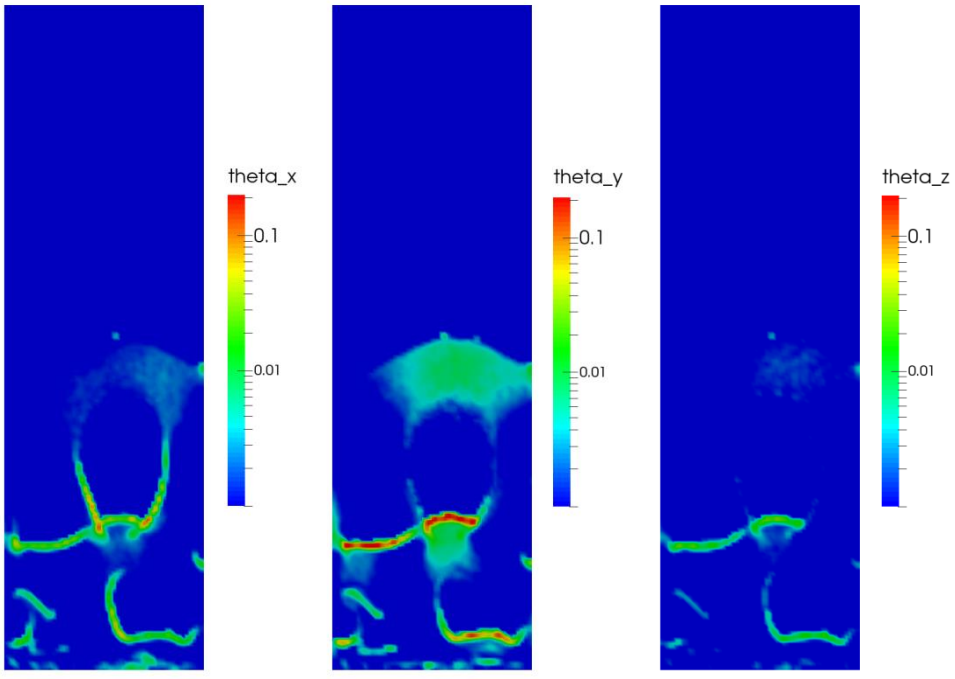

(a) (b) (c)

Figure 4. Components of granular temperature in (a) x, (b) y and (c) z directions. (Numerical simulation: U_g=0.88m/s, μ_{fric}=0.6).

Similar analysis is conducted for the tangential and normal wall stresses as shown in Figure 5. Again, the linear relationship has been obtained which is consistent with the standard friction equation. Hence, the slope of the fitted line can be interpreted as an effective coefficient of friction between the particles flow and wall.

$$T_s = \mu_{eff} T_n \tag{8}$$

The predicted effective friction coefficient of 0.2702 is lower than that of 0.6 for the particle and wall surface. According to the rigid-body theory, only two possible rebound behaviors corresponding to sliding and non-sliding collision exist for a rigid spherical body colliding with the wall [38]. For a sliding particle-wall collision, the normal and tangential forces can be described by the Coulomb law. For a non-sliding collision, the relative displacement of the contact point does not occur so that the sphere is rolling on

the surface during the contact which results in much lower friction comparing to the sliding collision. Hence the overall effective friction coefficient is lower than the coefficient of friction specified for the sliding particle-wall contact. The interaction between the particle flow and wall would be more complicated than depicted by the rigid body theory. The current DEM implementation is capable of capturing the aforementioned contacts which makes it an ideal tool for investigating the particle-wall interactions.

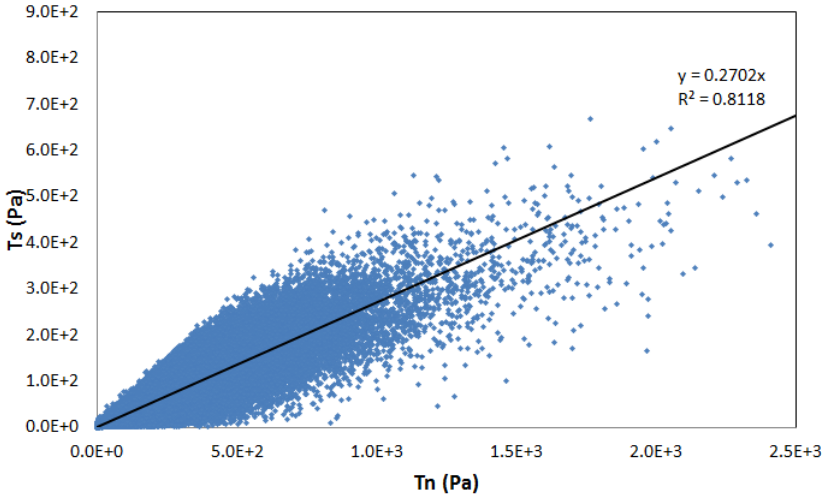

Figure 5. Tangential wall stress versus normal wall stress for the emulsion phase together with a linear regression (Numerical simulation: U_g=0.88m/s, μ_{fric}=0.6).

It should be noted that the effective friction coefficient derived from fitting the transient data fluctuates slightly. To obtain the representative relationship between normal and tangential forces, sufficient sample points are needed. Figure 6 shows the effective frictional coefficient obtained from different sample periods with the data saving frequency of 100 Hz. Typically, the data collected in 1~2 s after the flow is fully developed is believed sufficient for deriving the effective friction coefficient for the current system, considering the high number of data points obtained in each frame.

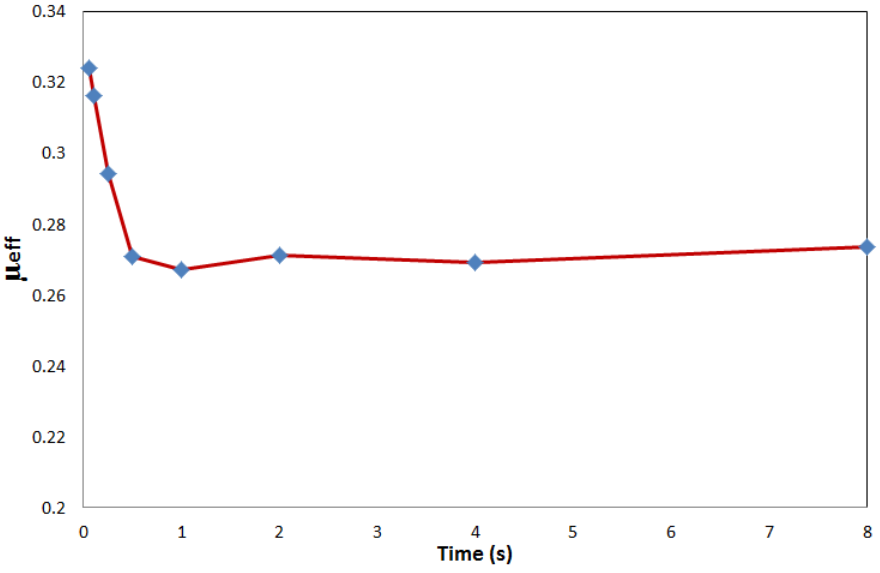

Figure 6. Effective frictional coefficient as a function of sample time period (Numerical simulation: U_g=0.88m/s, μ_{fric}=0.6).

3.3. Effective frictional coefficient

A parametric study of the friction coefficient has been conducted by varying it from 0.3 to 0.7. In the current study, the same friction coefficients are used for both particle-particle and particle-wall interactions since the bed material and wall material can be considered similar. Figure 7 plots the normal wall stress versus the solids pressure for the emulsion phase for simulations with different friction coefficients. For different conditions, the linear regression fits the data reasonably. The slopes of the linear fitting are close and no general trend can be obtained. The results tend to indicate the friction coefficient has no significant influence on the anisotropy in stress tensor.

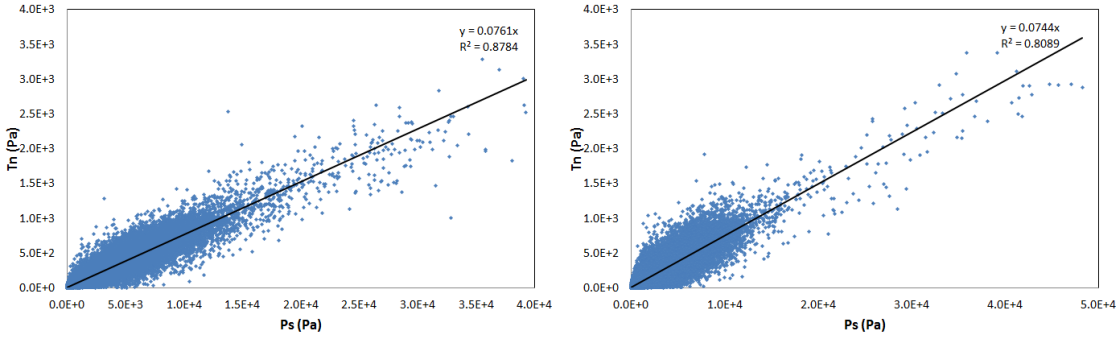

(a) (b)

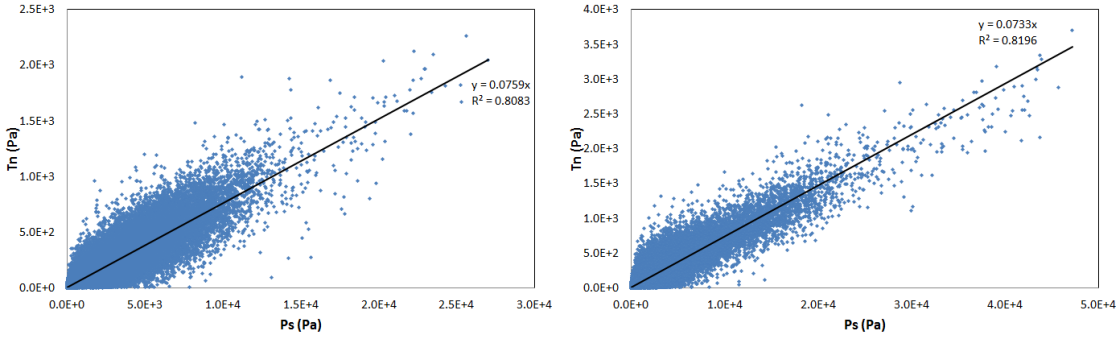

(c) (d)

Figure 7. Normal wall stress versus solids pressure for the emulsion phase together with a linear regression for different friction coefficients (a) μ_{fric}=0.3; (b) μ_{fric}=0.4; (a) μ_{fric}=0.5; (a) μ_{fric}=0.7.

Figure 8 shows the tangential wall stress versus the normal wall stress for different friction coefficients. As can be seen in the figure, the data points become more scattering as the friction coefficient increases. Overall, the linear relationship still reasonably describes the data though the reported R-Square value decreases with the increasing friction coefficient indicating less accuracy in the fitting. The slope of a linear fitting, i.e. the effective friction coefficient, increases as the particle-particle and particle-wall friction coefficient increases. For the current system, the effective friction coefficient increases from 0.23 to 0.28 as the particle-particle and particle-wall friction coefficient increases from 0.3 to 0.7. The slower increase in the effective friction coefficient suggests a moderate dependence on the friction coefficient.

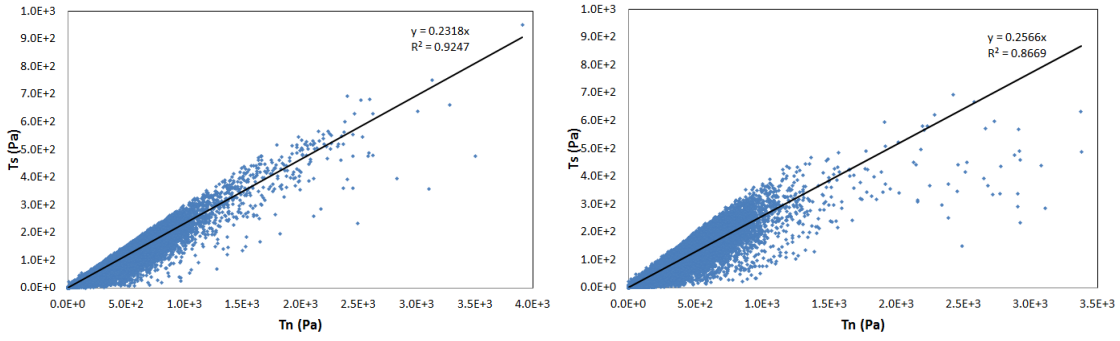

(a) (b)

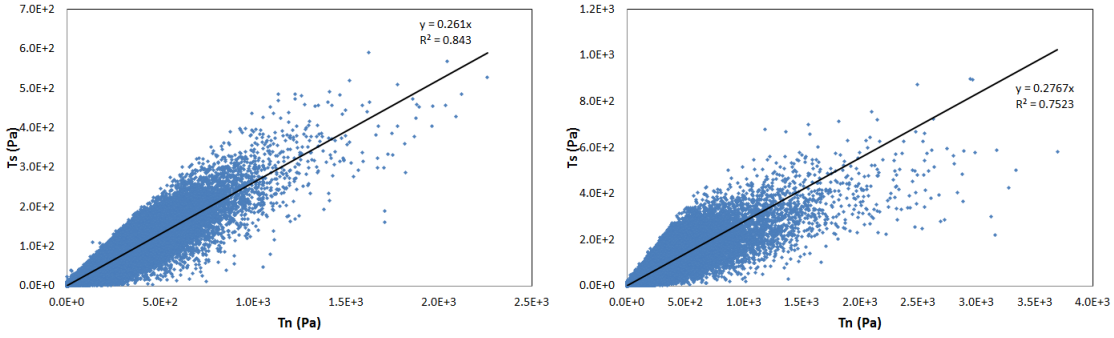

(c) (d)

Figure 8. Tangential wall stress versus normal wall stress for the emulsion phase together with a linear regression for different friction coefficients (a) μ_{fric}=0.3; (b) μ_{fric}=0.4; (a) μ_{fric}=0.5; (a) μ_{fric}=0.7.

3.4. Effect of spring constant

In the linear spring-dashpot soft-sphere model used in the current study, the time for particle collision is expressed as a function of particle size and hardness. To avoid extremely small time step for the simulation, a lower spring constant is typically used in the CFD-DEM simulations which usually does not affect the simulation results [30]. It has been a typical exercise to speedup DEM simulation by reducing the particle stiffness to make particles less stiff or softer to allow a larger time step [39]. On the other hand, some studies have suggested that reduction in particle stiffness can lead to undesirable effects. For example, properties such as the bulk stiffness and bulk restitution of granular flow changed as a result of the stiffness reduction [40]. The spring constant in the contact force model affects the rebound and sticking behavior of the collision of cohesive fine particles in gas-solid fluidized bed [41]. Hence, it is important to verify the simulation results are not affected by the particle stiffness substantially.

To investigate the effect of particle stiffness, two simulations with the normal spring constant of 20000 and 200000 N/m for particle-particle and particle-wall interactions were conducted for the friction coefficient of 0.6. It should be noted that as the spring constant increases, the duration of collision between two particles decreases proportionally to the square root of the spring constant. Hence the time step required for accurate resolution of particle contact has to be reduced which results in much longer CPU time. To alleviate the extreme computational cost associated with high spring constants, only 2 s simulations were completed by restarting from the run with the spring constant of 2000 N/m. The results of the last second are analyzed.

During the data analysis, it was found that the calculated field variables, i.e. solids pressure and wall stresses for the runs with high spring constants are highly dispersed comparing to the results shown above. After careful examination, it is determined that the default window of one fluid cell for analysis is not sufficient to derive the macroscopic field variable without significant statistical noise. This is mainly because of the less particle contacts captured by the instantaneous snapshot of the simulation due to the reduced duration of collision. On the other hand, the increased contact force between two colliding particles further introduces more statistical noises. To overcome this, the sampling window has been extended from 1 fluid cell to 2×2, 3×3 and 4×4 fluid cells. As shown in Figure 9, there exist more and more evident correlation between normal wall stress and the solids pressure as the sampling window is extended. The following results are based on the sampling window of 3×3 fluid cells.

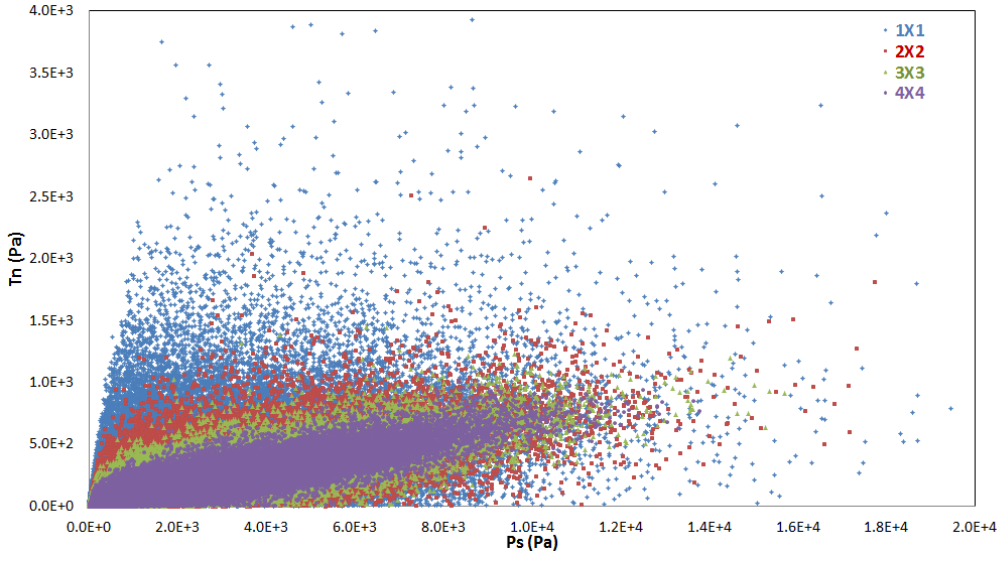

Figure 9. Normal wall stress versus solids pressure in the emulsion phase for the simulation with spring constant of 200000 N/m using different window sizes.

Figure 10 shows the relationship between solids pressure and normal wall stress as predicted by different spring constants using 3×3 fluid cells for analysis. As can be seen, the linear regression does a better job fitting the results for low spring constant in Figure 10(a) than that in Figure 3 as the increased window size reduce the statistical noise. The data become less correlated between solids pressure and normal wall stress for simulation with higher spring constants which is believed to be related to the statistical noise due to high particle stiffness. Overall, the linear regression fits all data reasonably well and the slopes remain almost constant for different values of particle stiffness.

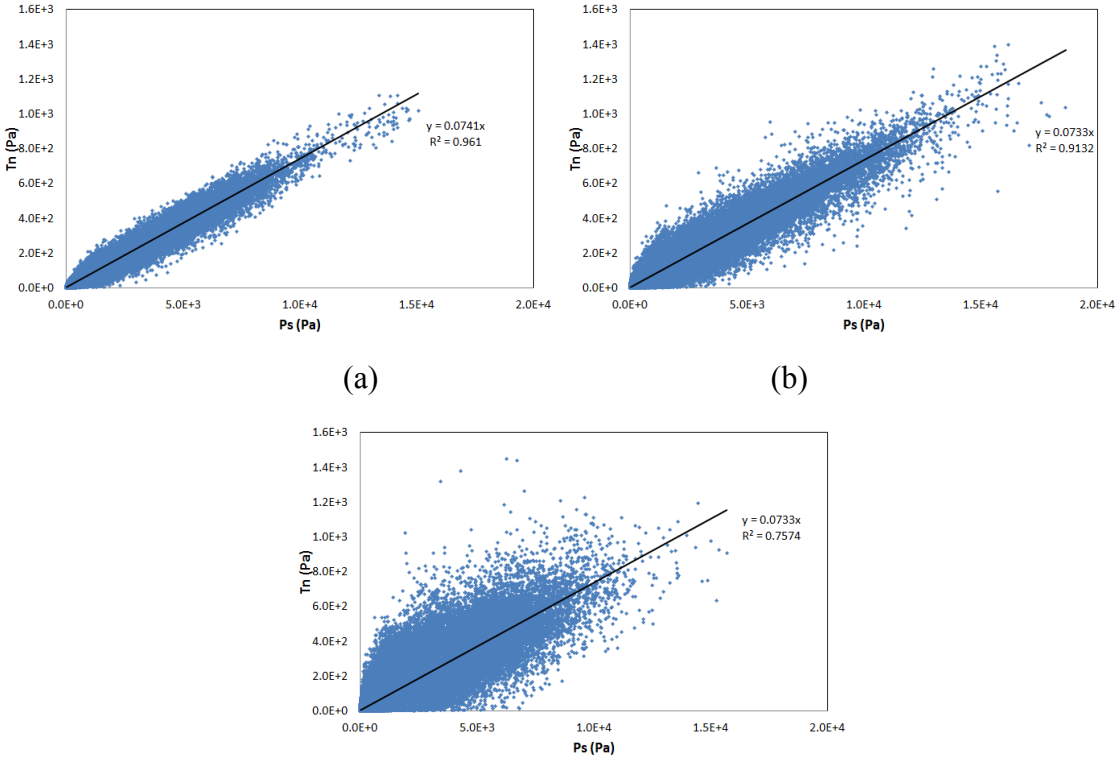

Figure 10. Normal wall stress versus solids pressure for the emulsion phase together with a linear regression for different spring constant (a) 2000 N/m; (b) 20000 N/m; (c) 200000 N/m.

Figure 11 shows the tangential wall stress versus the normal wall stress for simulations with different spring constants. Similarly, the data become less correlated for higher spring constants due to the increased statistical noise. Overall, the linear relationship can still reasonably describe all the data. The slope of a linear fitting, i.e. the effective friction coefficient, increases slightly as the particle spring constant is increased which suggests the particle stiffness does affect the particle-wall interaction. Attention on the particle stiffness is needed for the DEM study when accurate quantitative prediction on particle-particle and particle-wall interaction forces is sought.

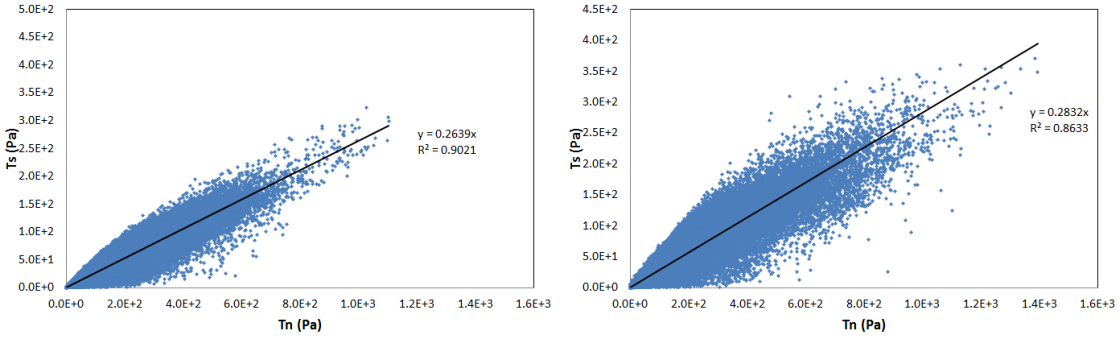

(a) (b)

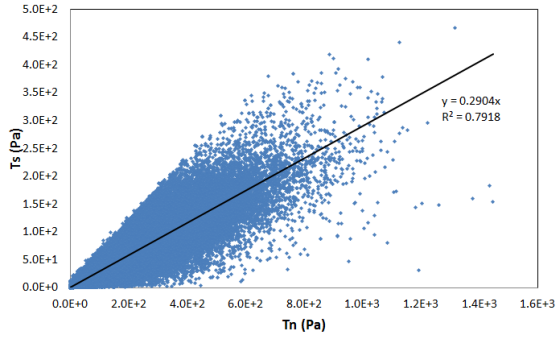

(c)

Figure 11. Tangential wall stress versus normal wall stress for the emulsion phase together with a linear regression for different spring constant (a) 2000 N/m; (b) 20000 N/m; (c) 200000 N/m.

3.5. Revisiting Li and Zhang's model

Li and Zhang [24] developed a 2D model for TFM simulations to account for the front and back wall effects in a pseudo-2D gas-solid fluidized bed. In this model, the collisions between particles and the front and back walls are assumed to be sliding. The shear stress S exerted by the wall is then calculated as

$$S = \mu N \tag{8}$$

where N is the normal wall stress. The normal wall stress is estimated from the solids pressure calculated in the 2D simulation. With the 2D flow assumption, the shear force imposed by the front and back walls can be interpreted as a body force acting on the solids flow.

The DEM simulation results here can be used to verify the assumptions used in Li and Zhang's model. Clearly, the normal wall stress is much lower than the solids pressure due to the strong anisotropic flow behavior. The anisotropy in solids stress should be considered when the solids pressure is used to approximate the normal wall stress. Furthermore, an effective friction coefficient should be used in equation (8) instead of the particle-wall friction coefficient. As demonstrated above, the effective friction coefficient is much lower than the particle-wall frication coefficient. On the other hand, there exists a linear relationship between the shear stress and the solids pressure which make it possible to account for the wall effect in a 2D simulation through a single parameter lumping the flow anisotropy and the effective friction coefficient together. However, one might need certain calibration steps to determine its appropriate value based on the experimental data.

4. Conclusion

For the pseudo-2D gas-solid system investigated, there exists a strong correlation between the normal stress and tangential stress at the wall in the dense emulsion phase. An effective frictional coefficient can be used to reasonably describe the relationship. The effective frictional coefficient is lower than the particle-wall frictional coefficient. It increases with the particle-wall frictional coefficient. There exist significant anisotropic behaviors in solids stress and granular temperature. The normal wall stress is much lower than the solids pressure and the granular temperature component in the thickness direction is lower than those in the other two directions. The assumptions in the 2D model for a pseudo-2D gas-solid system by Li and Zhang [24] are examined and the flow anisotropy and the effective friction coefficient are suggested to be considered in the model.

In the current CFD-DEM study, the spring constant, which characterizes the particle stiffness, affects the force analysis to certain extent although it does not alter the qualitative conclusion. Special attention is needed when using DEM to investigate the particle-particle and particle-wall interaction especially when the quantitative prediction is sought. Overall, CFD-DEM has been demonstrated a very useful tool for detailed investigation of gas-solids flow.

Nomenclature

$\boldsymbol{\sigma}$	stress	Pa
ε	volume fraction	-
μ	friction coefficient	-
ρ	density	kg/m^3
Θ	granular temperature	m^2/s^2
A	area	m^2
F	force	N
N	normal wall stress	Pa
P	pressure	Pa
S	tangential wall stress	Pa
T	stress	Pa
$\mathbf{u}$	velocity	m/s
U	velocity	m/s

V	volume	m^3

Acknowledgments

This technical report was produced in support of the National Energy Technology Laboratory's ongoing research in advanced numerical simulation of multiphase flow under the RES contract DE-FE0004000.

References:

[1] L.E. Rowe P.N., Partridge B.A., Cheney A.G., Henwood G.A., The mechanisms of solids mixing in fluidized beds, Trans. Institutetution Chem. Eng. 43 (1965) 271–286.

[2] K.S. Lim, P.K. Agarwal, B.K. O'neill, Measurement and modelling of bubble parameters in a two-dimensional gas-fluidized bed using image analysis, Powder Technol. 60 (1990) 159–171.

[3] G.R. Caicedo, J.J.P. Marqués, M.G. Ruíz, J.G. Soler, A study on the behaviour of bubbles of a 2D gas–solid fluidized bed using digital image analysis, Chem. Eng. Process. Process Intensif. 42 (2003) 9–14.

[4] A. Busciglio, G. Vella, G. Micale, L. Rizzuti, Analysis of the bubbling behaviour of 2D gas solid fluidized beds, Chem. Eng. J. 140 (2008) 398–413.

[5] M.J.V. Goldschmidt, J.M. Link, S. Mellema, J.A.M. Kuipers, Digital image analysis measurements of bed expansion and segregation dynamics in dense gas-fluidised beds, Powder Technol. 138 (2003) 135–159.

[6] W. Zhong, M. Zhang, Jet penetration depth in a two-dimensional spout–fluid bed, Chem. Eng. Sci. 60 (2005) 315–327.

[7] D. Pallarès, F. Johnsson, A novel technique for particle tracking in cold 2-dimensional fluidized beds—simulating fuel dispersion, Chem. Eng. Sci. 61 (2006) 2710–2720.

[8] C.R. Müller, J.F. Davidson, J.S. Dennis, A.N. Hayhurst, A Study of the Motion and Eruption of a Bubble at the Surface of a Two-Dimensional Fluidized Bed Using Particle Image Velocimetry (PIV), Ind. Eng. Chem. Res. 46 (2007) 1642–

[9] J.A. Laverman, I. Roghair, M. van S. Annaland, H. Kuipers, Investigation into the hydrodynamics of gas–solid fluidized beds using particle image velocimetry coupled with digital image analysis, Can. J. Chem. Eng. 86 (2008) 523–535.

[10] J. Xu, J.-X. Zhu, Visualization of particle aggregation and effects of particle properties on cluster characteristics in a CFB riser, Chem. Eng. J. 168 (2011) 376–389.

[11] F. Hernández-Jiménez, T. Li, E. Cano-Pleite, W. Rogers, A. Acosta-Iborra, Characterization of the particle–wall frictional forces in pseudo-2D fluidized beds using DEM, Chem. Eng. Sci. 116 (2014) 136–143.

[12] F. Hernández-Jiménez, S. Sánchez-Delgado, A. Gómez-García, A. Acosta-Iborra, Comparison between two-fluid model simulations and particle image analysis & velocimetry (PIV) results for a two-dimensional gas–solid fluidized bed, Chem. Eng. Sci. 66 (2011) 3753–3772.

[13] F. Hernández-Jiménez, J. Sánchez-Prieto, A. Soria-Verdugo, A. Acosta-Iborra, Experimental quantification of the particle–wall frictional forces in pseudo-2D gas fluidised beds, Chem. Eng. Sci. 102 (2013) 257–267.

[14] S. Sánchez-Delgado, C. Marugán-Cruz, A. Soria-Verdugo, D. Santana, Estimation and experimental validation of the circulation time in a 2D gas–solid fluidized beds, Powder Technol. 235 (2013) 669–676.

[15] E.D.J. Rowe P.N., Fluidised bed bubbles viewed by X-rays Part II- The transition from two to three dimensions of undisturbed bubbles, Chem. Eng. Res. Des. 50 (1972) 49–54.

[16] D. Geldart, The size and frequency of bubbles in two- and three-dimensional gas-fluidised beds, Powder Technol. 4 (1970) 41–55.

[17] R.R. Cranfield, D. Geldart, Large particle fluidisation, Chem. Eng. Sci. 29 (1974) 935–947.

[18] L.R. Glicksman, G. McAndrews, The effect of bed width on the hydrodynamics of large particle fluidized beds, Powder Technol. 42 (1985) 159–167.

[19] T. Kawaguchi, T. Tanaka, Y. Tsuji, Numerical simulation of two-dimensional fluidized beds using the discrete element method (comparison between the two- and three-dimensional models), Powder Technol. 96 (1998) 129–138.

[20] Y.Q. Feng, A.B. Yu, Effect of Bed Thickness on the Segregation Behavior of Particle Mixtures in a Gas Fluidized Bed, Ind. Eng. Chem. Res. 49 (2010) 3459–3468.

[21] T. Li, J. Grace, X. Bi, Study of wall boundary condition in numerical simulations of bubbling fluidized beds, Powder Technol. 203 (2010) 447–457.

[22] T. Li, P. Gopalakrishnan, R. Garg, M. Shahnam, CFD–DEM study of effect of bed thickness for bubbling fluidized beds, Particuology. 10 (2012) 532–541.

[23] S. Cloete, A. Zaabout, S.T. Johansen, M. van Sint Annaland, F. Gallucci, S. Amini, The generality of the standard 2D TFM approach in predicting bubbling fluidized bed hydrodynamics, Powder Technol. 235 (2013) 735–746.

[24] T. Li, Y. Zhang, A new model for two-dimensional numerical simulation of pseudo-2D gas–solids fluidized beds, Chem. Eng. Sci. 102 (2013) 246–256.

[25] M.A. van der Hoef, M. Ye, M. van Sint Annaland, A.T. Andrews, S. Sundaresan, J.A.M. Kuipers, Computational Fluid Dynamics, Elsevier, 2006.

[26] S. Chialvo, S. Sundaresan, A modified kinetic theory for frictional granular flows in dense and dilute regimes, Phys. Fluids. 25 (2013) 070603.

[27] M.Y. Louge, Computer simulations of rapid granular flows of spheres interacting with a flat, frictional boundary, Phys. Fluids. 6 (1994) 2253.

[28] R. Garg, J. Galvin, T. Li, S. Pannala, Documentation of open-source MFIX-DEM software for gas-solids flows. (2010). https://mfix.netl.doe.gov/documentation/dem_doc_2010.

[29] P.A. Cundall, O.D.L. Strack, A discrete numerical model for granular assemblies, Géotechnique. 29 (1979) 47–65.

[30] Y. Tsuji, T. Kawaguchi, T. Tanaka, Discrete particle simulation of two-dimensional fluidized bed, Powder Technol. 77 (1993) 79–87.

[31] R. Garg, J. Galvin, T. Li, S. Pannala, Open-source MFIX-DEM software for gas–solids flows: Part I—Verification studies, Powder Technol. 220 (2012) 122–137.

[32] T. Li, R. Garg, J. Galvin, S. Pannala, Open-source MFIX-DEM software for gas-solids flows: Part II — Validation studies, Powder Technol. 220 (2012) 138–150.

[33] H. Liu, D.K. Tafti, T. Li, Hybrid parallelism in MFIX CFD-DEM using OpenMP, Powder Technol. 259 (2014) 22–29.

[34] P. Gopalakrishnan, D. Tafti, Development of parallel DEM for the open source code MFIX, Powder Technol. 235 (2013) 33–41.

[35] S. Chialvo, J. Sun, S. Sundaresan, Bridging the rheology of granular flows in three regimes, Phys. Rev. E. 85 (2012) 021305.

[36] D. Gidaspow, Multiphase Flow and Fluidization: Continuum and Kinetic Theory Descriptions, Academic Press, 1994.

[37] B. Gopalan, F. Shaffer, Higher order statistical analysis of Eulerian particle velocity data in CFB risers as measured with high speed particle imaging, Powder Technol. 242 (2013) 13–26.

[38] T. Li, S. Benyahia, Revisiting Johnson and Jackson boundary conditions for granular flows, AIChE J. 58 (2012) 2058–2068.

[39] K.F. Malone, B.H. Xu, Determination of contact parameters for discrete element method simulations of granular systems, Particuology. 6 (2008) 521–528.

[40] S. Lommen, D. Schott, G. Lodewijks, DEM speedup: Stiffness effects on behavior of bulk material, Particuology. 12 (2014) 107–112.

[41] T. Kobayashi, T. Tanaka, N. Shimada, T. Kawaguchi, DEM–CFD analysis of fluidization behavior of Geldart Group A particles using a dynamic adhesion force model, Powder Technol. 248 (2013) 143–152.